Technical Report

INSTITUTES FOR ENVIRONMENTAL RESEARCH IER 43-ITSA 43

A Comparison of Sudden Ionospheric Frequency Deviations with Solar X-ray and Centimeter-Wave Emission During October 1963

DONALD M. BAKER

SEPTEMBER 1967

Boulder, Colorado

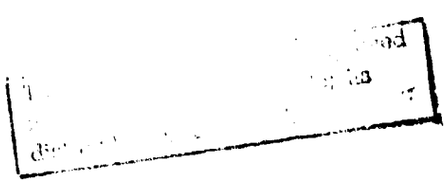

45

THE INSTITUTES FOR ENVIRONMENTAL RESEARCH

The mission of the Institutes is to study the oceans, and inland waters, the lower and upper atmosphere, the space environment, and the earth, seeking the understanding needed to provide more useful services. These research Institutes are:

- The Institute for Earth Sciences
  conducts exploratory and applied research in geomagnetism, seismology, geodesy, and related earth sciences.

- The Institute for Oceanography
  works to increase knowledge and improve understanding of the ocean and its interaction with the total physical environment of the globe.

- The Institute for Atmospheric Sciences
  seeks the understanding of atmospheric processes and phenomena that is required to improve weather forecasts and related services and to modify and control the weather.

- The Institute for Telecommunication Sciences and Aeronomy
  supports the Nation's telecommunications by conducting research and providing services related to radio, infrared, and optical waves as they travel from a transmitter to a receiver. The Institute is also active in the study and prediction of periods of solar activity and ionospheric disturbance.

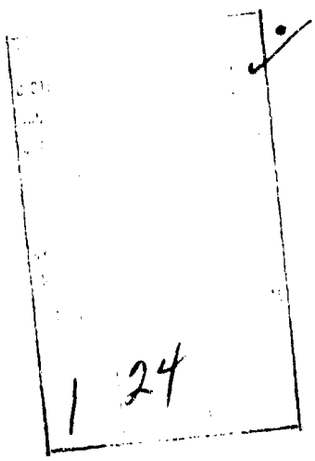

Environmental Science Services Administration

Boulder, Colo.

U. S. DEPARTMENT OF COMMERCE
Alexander B. Trowbridge, Secretary
ENVIRONMENTAL SCIENCE SERVICES ADMINISTRATION
Robert M. White, Administrator
INSTITUTES FOR ENVIRONMENTAL RESEARCH
George S. Benton, Director

ESSA TECHNICAL REPORT IER 43-ITSA 43

A Comparison of Sudden Ionospheric Frequency Deviations with Solar X-ray and Centimeter-Wave Emission During October 1963

DONALD M. BAKER

This work was supported by the Advanced Research Projects Agency; Nuclear Test Detection Office under ARPA Order No. 183.

INSTITUTE FOR TELECOMMUNICATION SCIENCES AND AERONOMY
BOULDER, COLORADO
September, 1967

For sale by the Superintendent of Documents, U.S. Government Printing Office, Washington, D.C., 20402
Price 30 cents.

Contents

List of Figures

Abstract

A simple model is developed which permits us to calculate the sudden ionospheric frequency deviation which would be caused by a known solar X-ray burst, or vice-versa, to calculate the time profile of the X-ray burst responsible for an observed frequency deviation. This model is also used to compare the frequency deviations observed during six solar flares with the time profiles of the solar emissions at centimeter and X-ray (0.5-10 Å) wavelengths which accompanied the flares.

Better time and spectral resolution are needed in order to permit a detailed comparison of the variations in the X-ray flux with the ionospherically induced frequency deviations.

Key Words: ionosphere, solar flare, solar X-ray emission, sudden frequency deviation (SFD), sudden ionospheric disturbance, solar radio emission

A COMPARISON OF SUDDEN IONOSPHERIC FREQUENCY DEVIATIONS WITH SOLAR X-RAY AND CENTIMETER-WAVE EMISSION DURING OCTOBER 1963

by

Donald M. Baker

1. Introduction

This report presents a study of the relationship between the radio and X-ray emissions of solar flares and the ionospheric disturbances called sudden frequency deviations (SFD). Since the X-ray bursts which accompany many solar flares are absorbed in the earth's atmosphere, we can use ground-based radio techniques to detect these X-ray bursts. However, in the past few years solar X-ray emission has been monitored directly by several artificial satellites (Bowen et al., 1964; Chubb, Friedman, and Kreplin, 1964; Conner et al., 1964; Friedman, 1964; Pounds, 1965). These satellite observations offer us an opportunity for studying the relationship between the ionizing radiation and the resulting disturbances of ionospheric radio propagation, such as sudden phase anomalies (SPA), short wave fadeouts (SWF), and sudden frequency deviations (SFD). Such studies are needed if ground-based radio techniques are to be used as tools to investigate the physics of the ionospheric response to solar ionizing radiations or if these techniques are to be used to study the nature of the radiation bursts themselves.

There is evidence that solar radio bursts at centimeter wavelengths and X-ray bursts are very closely related (Kundu, 1965). This makes a comparison of the ionospheric effects of solar flares with both the X-ray and associated centimeter-wave radio emissions desirable.

In this report we will restrict ourselves to a study of the relationship between sudden frequency deviation and the associated X-ray and centimeter radio bursts. In section 2 we develop a simple theory useful in the interpretation of a sudden frequency deviation and use this theory to calculate the shapes of the frequency deviations which would be produced by various time profiles for the ionizing radiation burst. In section 3 we compare the sudden frequency deviations, centimeter-wave radio emissions, and the X-ray bursts observed by the Vela satellites for the six solar flares listed in table 1. A description of the data used is given below.

Table 1

Optical ($H\alpha$) Observations of Solar Flares Discussed in Section 3
(E = before, D = later than)

Date	Time (UT) Beginning	Maximum	End	Importance
Oct. 18, 1968	[illegible]	[illegible]	[illegible]D	1+
[illegible]	[illegible]	[illegible]	[illegible] D	[illegible]
[illegible]	[illegible]	[illegible]	[illegible]D	[illegible]
[illegible]	[illegible]	[illegible]	[illegible]	1
[illegible]	[illegible]	[illegible]	[illegible] D	[illegible]
[illegible]	[illegible]	[illegible]	[illegible]	[illegible]
[illegible]	[illegible]E	[illegible]	[illegible]	[illegible]

4.1. Vela Satellite Data

The first pair of Vela satellites was launched in October 1963 into nearly circular orbits of approximately one-fourth and 4-hr period. The two spacecraft were given an angular separation of about 120°. The large orbits and the separation of the spacecraft permitted the sun to be monitored almost continuously. Each satellite has a spin rate of about 120 rpm. The X-ray detectors (two per satellite) were arranged so that several of them would be pointed sunward regardless of the orientation of the satellites. The detectors were sensitive to two overlapping spectral bands: 2 to 10 Å and 0.2 to 4 Å.

The X-ray data shown in the figures of this report correspond to the energy which was absorbed in the detector and not the incident flux. However, provided that the spectral characteristics of the flux did not change drastically during a burst, the data should give at least a rough picture of the time variation of the incident flux. The detector output was compared with a series of seven reference levels, and the highest level exceeded was recorded at the ground. Thus, the data received at the ground were quantized into discrete levels, resulting in a stair-step profile when the flux is plotted as a function of time. The detectors had a threshold of [illegible] ergs cm^{-2} sec^{-1} and became saturated when the absorbed flux reached [illegible] ergs cm^{-2} sec^{-1}. Details of the spacecraft and the detectors are given by Conner et al. (1965).

1.2. Centimeter Radio Data

The radio data consist of fixed frequency observations at centimeter wavelengths made at Ottawa, Ontario (2800 Mc/s) (Covington and Harvey, 1958; Harvey, 1964) and Toyokawa, Japan (200, 3750, and 9400 Mc/s) (Tanaka and Kakinuma, 1958). The events used in this report have been replotted from copies or tracings of the original records.

1.3. Ionospheric Disturbance Data

The ionospheric disturbance data consist of variations in the received frequency of high-frequency ionospherically propagated radio signals. These data are obtained by the Doppler technique described by Watts and Davies (1960) which detects rapid changes in the electron content of the ionosphere up to the level of reflection.

The frequency of an ionospherically propagated HF radio signal usually shows small variations (of the order of a few tenths of a cycle per second) about the transmitted frequency. However, during some natural phenomena, such as solar flares and geomagnetic sudden commencements, the received frequency often shows large (up to tens of cycles per second) and quite distinctive variations from the transmitted frequency. These flare-related frequency deviations have been given the name sudden frequency deviations (SFD) (Chan and Villard, 1963). Studies by Donnelly (1966); Agy, Baker, and Jones (1965); Davies, Watts, and Zacharisen (1962); and Kanellakos, Chan, and Villard (1962) indicate that they are caused by an increase of ionization in the E and/or F regions of the ionosphere. Details of the technique and the interpretation of the records can be found in Davies and Baker (1966) and Donnelly (1966) and the references contained therein.

2. Theoretical Discussion

2.1. Basic Equations and Model Used

If a radio wave of carrier frequency f propagates through a changing ionosphere, it will suffer a change in frequency, or Doppler shift, Δf given by

$$\Delta f = - \frac{f}{c} \frac{dP}{dt} \quad , \qquad (1)$$

where c is the speed of light in vacuum. The phase path of propagation, P, is given by

$$P = \int_{path} \mu ds \quad , \qquad (2)$$

where, neglecting the effects of the geomagnetic field and collisions,

$$\mu = \sqrt{1 - \frac{kN}{f^2}} \qquad (3)$$

is the refractive index. Here $k = 8 \times 10^{-6} \left(\frac{Mc}{s}\right)^2 cm^3$, the electron density N is in cm^{-3}, and the wave frequency f is in Mc/s.

Using (2) and (3), Agy, Baker, and Jones (1965) have shown that (1) can be written

$$\Delta f = \frac{k}{2fc} \int_{path} \frac{\frac{\partial N}{dt}}{\mu} \, ds \quad . \qquad (4)$$

If the changes causing Δf are confined to a non-deviating region where $\mu \approx 1$ (i.e., a region below the height of reflection)

$$\Delta f = \frac{kn}{fc} \int_{\text{ground}}^{\text{reflection}} \frac{\partial N}{\partial t}\, ds$$

$$= \frac{kn}{fc} \frac{dN_T}{dt} \quad , \tag{5}$$

where

$$\frac{dN_T}{dt} \equiv \int_{\text{ground}}^{\text{reflection}} \frac{\partial N}{\partial t}\, ds \tag{6}$$

is the rate of change of the total electron content and n is the number of ionospheric reflections. Therefore, when ionospheric changes are confined to a region below the reflection height of the radio wave being monitored, the Doppler shift observed will be directly proportional to the total time rate of change of electron content along the propagation path. In the ionospheric changes extend all the way to the height of reflection and if there is no major change in the propagation path (such as a change from F-layer to E-layer reflection), we would expect from (4) that the shape of $\Delta f(t)$ would still reflect the major time variations of the total electron content along the path; however, the magnitude of $\Delta f(t)$ will now be influenced by the variation of μ along the path. Henceforth, we will consider only the non-deviative model.

The time rate of change of the electron density in a region in which the electron loss processes can be described by an effective recombination coefficient α is given by

$$\frac{dN}{dt} = q - \alpha N^2 \quad , \tag{7}$$

where q is the electron production rate. Assume that the electron pro-

duction and loss rates are in equilibrium before a solar flare. Then, if the production rate and electron density are increased by amounts $\Delta q(t)$ and $\Delta N(t)$ during a flare (i.e., $q(t) = q_o + \Delta q(t)$, $N(t) = N_o + \Delta N(t)$ where the zero subscripts denote the equilibrium values), (7) can be written as

$$\frac{dN}{dt} = \frac{d\Delta N}{dt} = \Delta q - 2\alpha N_o \Delta N \left(1 + \frac{\Delta N}{2N_o}\right) \qquad (8)$$

or

$$\frac{d\Delta N}{dt} = \Delta q - \frac{\Delta N}{\tau}\left(1 + \frac{\Delta N}{2N_o}\right) , \qquad (9)$$

where τ is defined as

$$\tau = \frac{1}{2\alpha N_o} . \qquad (10)$$

Integration of (9) over the same integration path used to obtain (5), assuming that the region affected by the flare can be characterized by constant α and N_o, yields

$$\frac{d\Delta N_T(t)}{dt} = \Delta q_T(t) - \frac{\Delta N_T(t)}{\tau}\left(1 + \frac{\Delta N_T(t)}{2N_o}\right) , \qquad (11)$$

where the time dependence is now indicated explicitly. This equation, when combined with (5), allows us to synthesize the Δf to be expected from a known or assumed $\Delta q_T(t)$, or to deduce the $\Delta q_T(t)$ responsible for an observed $\Delta f(t)$. Moreover, since the frequency deviations caused by flares rarely last more than a few minutes, the solar zenith angle is essentially constant during such an event, and the electron production rate in a given region should closely follow the flux of the ionizing radiation enhancement. Hence, if the major flare effects detected by the Doppler technique do

indeed take place below the height of reflection, the simple model developed here should permit us to determine the time profile of the burst of ionizing radiation causing an ionospheric disturbance.

When $\Delta N \ll 2N_o$, (11) can be solved analytically for $d\Delta N_T/dt$. This is most easily done by differentiating (11) with respect to time and solving the resulting second order equation for $\Delta\dot{N}(t)$, where we now let the dot stand for the time derivative. The result gives:

$$\Delta\dot{N}_T(t) = e^{-\frac{t}{\tau}}\left[\int e^{\frac{t}{\tau}}\ \Delta\dot{q}_T(t)dt + \frac{C}{\tau}\right], \qquad (12)$$

where C is a constant of integration. This last expression can be stated in terms of $\Delta q_T(t)$ instead of $\Delta\dot{q}_T(t)$ by integrating by parts:

$$\Delta\dot{N}_T(t) = \Delta q_T(t) - \frac{e^{-\frac{t}{\tau}}}{\tau}\left[\int \Delta q_T(t)\, e^{\frac{t}{\tau}}\, dt - C\right]. \qquad (13)$$

If $\Delta q_T(t)$ and the appropriate value of τ are known, (13) enables $\Delta\dot{N}_T(t)$, and hence $\Delta f(t)$, to be calculated. Under these conditions (i.e. $\Delta N \ll 2N_o$), τ can be considered as an effective relaxation time of the ionosphere.

Alternatively, the $\Delta q_T(t)$ responsible for an observed $\Delta f(t)$ can be obtained by substituting (6) into (11) to obtain the following expression for $\Delta q_T(t)$ in terms of $\Delta f(t)$:

$$\Delta q_T(t) = \frac{fc}{k}\left\{\Delta f(t) + \frac{1}{\tau}\int_o^t \Delta f(x)dx\left[1 + \frac{fc}{2N_o k}\int_o^t \Delta f(x)dx\right]\right\}, \qquad (14)$$

where x is a variable of integration.

Examples of both of these approaches will be given in section 3, where the frequency disturbances are compared with the X-ray bursts in the 0.5- to 10-Å ranges observed by the Vela satellites.

2.2 Model Calculations

Five simple models of the enhancement of the electron production rate, $\Delta q_T(t)$, are shown in figures 1(a), 1(c), and 1(e) and in figures 2(a) and 2(c). The frequency deviations caused by these production rate enhancements were calculated from (13) using assumed values of the effective relaxation time, τ, of 0.5, 1, 5, and 10 min. Three simple models of $\Delta q_T(t)$ are shown in figure 1. An impulsive rise to a peak followed by a slower decay to the undistrubed level (fig. 1a) causes a positive frequency deviation followed by a negative shift and a gradual recovery to the undisturbed frequency (fig. 1b). A rapid rise of electron production rate to a new constant level (fig. 1c) causes a rapid frequency increase and a gradual recovery to the undisturbed frequency with no negative phase (fig. 1d). A gradual rise and fall of the electron production rate (fig. 1e) results in a small and gradual increase in frequency followed by a small negative deviation and a gradual recovery (fig. 1f). Frequency deviations similar to those in figures 1(b) and 1(d) have been observed frequently during solar flares. Effects similar to those of figure 1(f) have also been observed; however, such small, gradual frequency variations are hard to distinguish from the normal background variations which are usually present, and up to now they have not been considered as flare-related events. In the past the rapidity of a frequency

deviation has been one of the criteria used to recognize a sudden frequency deviation; the present study suggests that such a criterion may result in many flare-related events being missed. However, the Doppler technique is not suitable for quantitative study of these gradual events.

Slightly more complex electron production rate enhancements are shown in figures 2(a) and 2(c). Figure 2(a) shows a Δq with a double rise, the two increases being separated by a short period during which the production rate remains at a constant but enhanced level. For the shorter relaxation times such a model leads to a frequency deviation having two distinct peaks (fig. 2b), which become less pronounced as the relaxation time increases. An impulsive burst superimposed upon the initial part of a gradual rise and fall is shown in figure 2(c). This production rate model causes an initial frequency deviation similar to that caused by a simple impulsive burst (fig. 1a and 1b); however, for the shorter relaxation times the gradual increase in the production rate following the impulsive burst shortens the length of the negative deviation and causes a second positive frequency shift similar to that caused by a simple gradual rise and fall of the production rate (fig. 1e and 1f). This "overshoot" is followed by a small negative deviation and a gradual recovery. For the longer relaxation times the gradual rise of the production rate prevents the frequency deviation from reaching the initial negative phase.

Many of the flare-related frequency disturbances observed have more than one peak and must be caused by complex bursts of ionizing radiation. Figures 2(a) and 2(b) indicate that if the effective relaxation time is smaller than or comparable to the time between rapid flux changes (about

1 min in this example) the burst of ionizing radiation need not have distinct peaks but merely needs to be made up of rapid flux increases separated by plateaus in order to cause distinct peaks in the frequency deviation. Frequency disturbances made up of a main deviation followed by an overshoot such as those of figure 2(d) have also been observed. Clearly, such events could be caused by an impulsive burst of ionizing radiation superimposed upon a gradual rise and fall similar to the production rate model of figure 2(c).

Comparison of the frequency deviations for the different relaxation times and the appropriate enhancements of the electron production rate in figures 1 and 2 shows (see (9)) that the frequency variation follows the enhancement of electron production rate more closely as the effective relaxation time becomes larger. The frequency deviation can depart significantly from the shape of the enhancement of the production rate for small relaxation times. Also, a negative frequency deviation is to be expected only when the production rate (i.e., the ionizing flux) decreases with time.

3. Specific Events

In this section we compare the X-ray bursts, radio bursts, and frequency deviations observed during the flares listed in table 1. The times of onset, durations, and general behavior of the three phenomena are investigated first. The shape of the frequency deviation to be expected from the 0.5- to 10-Å X-ray burst of October 22 is then calculated. Finally, the time profiles of the enhancements of electron production rate are deduced and compared with the X-ray observations.

3.1. Comparison of Observed X-ray Bursts, Solar Radio Bursts, and Frequency Deviations

The time variations of the X-ray flux in the 0.5- to 4-Å and 0.5- to 10-Å ranges, the solar radio flux at fixed frequencies in the centimeter wavelength region, and the frequency deviation of WWV (or WWVH) as received at Boulder are shown in figures 3 through 8. The radio flux is given in flux units (1 flux unit = 10^{-22}, W m^{-2} cps^{-1}), the frequency deviation in cycles per second, and the X-ray flux deposited in the detector in ergs cm^{-2} sec^{-1}. Note that the X-ray flux scale is linear. The 0.5- to 10-Å detectors became saturated during all but the 2240 event of October 22; the 0.5- to 4-Å detectors were saturated only during the October 18 event. The 4-min gaps in the Doppler data which occur at 45 min past the hour are due to the hourly WWV transmission break. The lowest level shown for the X-ray flux, about 1×10^{-3} ergs cm^{-2} sec^{-1}, represents the detector threshold and is not necessarily the background level. The radio and Doppler data have been scaled and replotted from copies of the original records; the timing is judged to be accurate to within a minute or better. The timing of the plots of the X-ray data may be off as much as 5 min.

Comparison of the observed 0.5- to 10-Å X-ray, centimeter radio, and frequency variation data for the six events leads to the following general observations:

1. To within the timing accuracy available, the onset times of the impulsive radio bursts and the frequency deviations are in agreement.
2. The X-ray flux usually increases rapidly during the impulsive radio bursts and the frequency deviations. The

Doppler technique tends to "see" the initial fast rise of the X-ray flux.

3. In the case of four of the five events for which radio data are available the duration of the frequency deviation is comparable to that of the impulsive radio burst; for the fifth event (fig. 5), the impulsive radio burst lasts longer than the frequency deviation.

4. For some events (figs. 3 and 6) the duration of the X-ray burst is of the same order as that of the frequency deviation; during other events (figs. 4,5,7, and 8) the X-ray flux remains at an enhanced level long after the frequency disturbance has ended.

5. No significant frequency deviations are observed during the (apparently) rapid decay of a long enduring X-ray burst. However, the exact beginning time and rate of decay of the recovery phase of such a burst cannot be determined due to the saturation of the detectors.

6. The radio bursts and frequency deviations often show fine structure--rapid, short duration variations. If radiation in the 0.5- to 3-Å range is the cause of the frequency deviations, we would expect corresponding fine structure to be present in the X-ray flux (Baker, Davies, and Grimes, 1966). However, the variation of the flux needed to produce the observed fine structure of the frequency deviations is probably too small to be detected by the instrumentation of the Vela satellites.

3.2. Calculation of the Frequency Deviation Expected from the X-ray Burst Observed at 2240 U.T. on 22 October 1963

Equation (13) of section 2 permits us to calculate the frequency deviation which will be caused by a given enhancement of the electron production rate. In deriving (13) we assume that the changes responsible for the frequency deviation are confined to a limited portion of the ionosphere which is non-deviative for the radio frequencies used. This effectively limits the changes to the E region and lower part of the F region for observations made at 10 and 15 Mc/s. We also assume that the electron loss processes in this region can be represented by an effective relaxation time, τ, which is essentially constant with height and for times of the order of the duration of the frequency deviation of interest. For a region where recombination loss processes predominate, this assumption requires that the increase in electron density caused by the flare be small compared with the ambient electron density. Donnelly (1966) has shown that X-radiation at wavelengths around 10 Å produces ionization mostly in the 90- to 110-km region. This level is well below the height of reflection (i.e., is non-deviative) for F-layer propagation of 10 to 15 Mc/s from WWV (Beltsville, Maryland) to Boulder, Colorado. (Both E- and F-layer propagation are received, but all the frequency deviations we will discuss were observed on signals propagated by the F-layer.) Therefore, the model used to derive (13) may not be too unrealistic, as far as the non-deviative assumption is concerned, for predicting the effects of ionizing radiation of about 10-Å wavelength. At these wavelengths the applicability of the model will be limited by the assumed constancy of τ and N_e with height. To calculate the shape of the fre-

quency deviation to be expected from a given X-ray burst, we will assume that the enhancement of the electron production rate has the same time profile as the X-ray burst.

The results of applying this technique to the 0.5- to 10-Å X-ray event observed by the Vela satellites at 2240 U.T. on 22 October 1963 are shown in figure 9. The "stair-step" profile of the burst shown in figure 6(c) has been smoothed as shown in figure 9(a). This profile was then used for $\Delta q_r(t)$ in (13), and the frequency deviation was calculated for effective relaxation times of 0.5, 1, and 5 min. The results are shown by the dotted curves of figures 9(b), 9(c), and 9(d); the solid curve shows the observed frequency shift for comparison. The times of the calculated and observed peaks have been aligned and the calculated peaks have been normalized to agree with the maximum observed deviation. There is some evidence that the X-ray peak occurred about 1 min after the peak frequency deviation (see fig. 12); however, this difference is well within the accuracy with which the records are timed and for the purposes of this calculation the peaks were assumed to occur at the same time.

From figures 9(c) and 9(d) we see that the gross features of the observed and calculated frequency deviations are in good agreement for relaxation times between 1 and 5 min. The detail of the decay is not reproduced, but this can hardly be expected since the profile in figure 9(a) had to be reconstructed from that of figure 6(c). Hence, we conclude from this study of the shapes that the X-ray burst observed by the Vela satellites could have produced the observed frequency deviation. We have said nothing about the magnitudes. In a more detailed study of this event,

Donnelly (1966) has found that the magnitude of the flux enhancement in the 0.5- to 10-Å range is not sufficient to produce the observed frequency deviation. He concludes that the frequency deviation must be at least partly a result of enhancements at longer wavelengths.

Since the flux exceeded the saturation level during a major portion of the other events observed at Boulder, it is not worthwhile to reconstruct the flux profile and calculate the frequency deviations which would be produced.

3.3. Synthesis of Profiles of the Enhancement of Electron Production Rate

In this section we take the observed frequency deviations as the input data and use (14) to calculate the enhancement of the electron production rate. The resulting profiles for effective relaxation times of 0.5, 1, and 10 min, shown in part (b) of figures 10 through 14, are compared with the observed 0.5- to 10-Å X-ray flux shown in part (c) of these figures.* The time scale of these figures is much expanded over that used in figures 3 through 8, and only the initial portion of each X-ray event is shown. After the initial peak frequency deviation and the initial part of the negative shift, the flare-related frequency deviation is usually lost in the background variation of the frequency; in making the calculations for figures 10 through 14, only that portion of a frequency deviation which could be reliably attributed to the flare was used.

---

*In calculating the enhancement of the electron production rate we have used a value of 10^{11} m^{-3} for N_o.

The curves of figures 10 through 14 show the shape of the electron production rate enhancement which would be needed to produce the observed frequency deviation for the simple model we have adopted. Comparison of the production rate enhancements with the X-ray fluxes must of necessity be qualitative due to the nature of the data available; our knowledge is limited by the saturation of the X-ray detectors, the lack of fine structure in the X-ray observations and the limited portion of the production rate profile which we can reconstruct from the frequency variation data. The most we can hope to conclude is whether or not the calculated production rate enhancement is compatible with the X-ray observations.

Smith, Accardo, Weeks, and McKinnon (1965) have concluded from recent eclipse observations that the effective daytime relaxation time in the E region is about 1 min. In addition, Baker and Davies (1966) have presented evidence that suggests that the effective daytime relaxation time in the region where the bulk of the ionization responsible for flare-related frequency deviations is released may be less than 1 min. Therefore, the most appropriate curves for the enhancement of electron production rate for the model we have adopted are probably those for an effective relaxation time of about 1 min.

Examination of figures 10 and 11 reveals that the synthesized production rate enhancement curves and the initial part of the X-ray burst are compatible for these two events. From a cursory inspection it may appear that the production rate curve is decaying faster than the X-ray flux, but closer inspection reveals that at the end of the records shown in the figures, the production rates are still above the levels they

had attained at the time the X-ray detectors became saturated. The production rate curves for these two events also show that the fine structure in the ionizing radiation needed to produce the fine structure of the frequency deviations is indeed small, especially if the effective relaxation time is short, and such small relative flux variations may prove to be hard to detect with satellite-borne instrumentation.

Figure 12 shows the curves for the 2240 October 22 event which was discussed in section 3.2. The time disagreement between the X-ray burst and the frequency deviation which was mentioned previously is shown in this figure. Here we will adopt the viewpoint that this discrepancy is within the accuracy to which the data can be timed and will assume that the two events are time coincident. Doing so, we see that the production rate curves for the shorter relaxation times are not compatible with the X-ray observations; indeed, the production curves decay much more slowly than the X-ray flux. The production rate curve for a relaxation time of 10 min is in fairly good qualitative agreement with the X-ray flux curve; this we would expect from the results of section 3.2 where we found that a relaxation time greater than 1 min was needed to make the frequency deviation calculated from the X-ray flux agree with the observed event.

The initial part of the event of October 26 is shown in figure 13. Only the two prominent frequency deviations at 1840 and 1902 were considered in calculating the enhancement of the electron production rate; the data between these two deviations were smoothed as indicated by the dashed lines. From the portion of the event shown, the production rate

enhancement and the X-ray burst appear to be compatible. However, the X-ray detectors had not yet reached saturation at 1908, and an abrupt increase to the saturation level shortly after 1908 caused no measurable frequency deviation. This fact forces us to question whether the 0.5- to 10-Å X-ray flux was responsible for the frequency deviations before 1908.

The electron production rate enhancement calculated for October 28 (fig. 14) does not agree in time with the X-ray flux enhancement. The production rate has peaked and is beginning to decay before the X-ray detectors become saturated. A shift of about 4 min would be necessary to make the production rate curve compatible with the X-ray burst; again such a shift is within the timing accuracy available.

From figures 10 through 14 we see that in some cases the X-ray flux in the 0.5- to 10-Å range could have caused an enhancement of the electron production rate of the shape needed to give the observed frequency variation, and that in other cases it could not. It may be significant that for the one event during which the X-ray detectors were not saturated (fig. 12), the production rate enhancement calculated for the shorter relaxation times, which we would expect to be operative in the E region where our model is applicable, differs appreciably from the X-ray burst. As pointed out by Donnelly (1966), the 0.5- to 10-Å flux may have contributed to the post-peak hump in the frequency variation while the main deviation was caused by enhancements at wavelengths greater than 10 Å.

4. Discussion

We cannot establish by a comparison of the time profiles of the data available whether or not X-ray bursts in the 0.5- to 10-Å range were sufficient to cause the frequency deviations observed during the solar flares of October 1963. To compare the frequency deviations and X-ray data, we have assumed that the spectral composition of the X-ray burst did not change during the burst. Some of the disagreement we have found may arise because the spectral characteristics of an X-ray burst do change rapidly with time. In any case, we could not definitely conclude that the frequency variations were or were not caused by the 0.5- to 10-Å X-rays from a study of time profiles alone without knowledge of the flux variations at longer wavelengths. Donnelly (1966) has concluded that the frequency deviations must be at least partly a result of enhancements at wavelengths greater than 10 Å.

Such a simple treatment of the data does reveal some worthwhile observations, however. We see that better timing accuracy is required for detailed comparison of the various data; such timing accuracy is now available on the Doppler data. Attempts should be made to obtain more detailed time profiles and better spectral resolution of solar X-ray bursts. Although the calculated enhancements of the electron production rate indicate that the fine structure necessary to produce the detail observed in the frequency deviations may be only a very small modulation of the main enhancement, the close correspondence which often exists between the frequency variations and the impulsive centimeter radio bursts suggests that similar impulsive bursts may exist in the flux of ionizing

radiation. Better spectral resolution and broader spectral coverage are needed to help us determine what wavelength regions produce the ionization enhancements responsible for the frequency variations and the height of these enhancements.

5. Acknowledgments

The X-ray data used in this study were furnished by Dr. Jerry P. Conner of the Los Alamos Scientific Laboratory; the radio data were supplied by A. E. Covington of the Radio and Electrical Engineering Division of the National Research Council of Canada and by Professor H. Tanaka of the Research Institute of Atmospherics of Nagoya University, Toyokawa, Japan. This work was supported by the Advanced Research Projects Agency, Nuclear Test Detection Office under ARPA Order No. 183.

6. References

Agy, V., D. M. Baker, and R. M. Jones (1965), Studies of solar flare effects and other ionospheric disturbances with a high frequency Doppler technique, NBS Technical Note No. 306 (U.S. Government Printing Office, Washington, D.C.).

Baker, D. M. and K. Davies (1966), Solar flare effects and the relaxation time of the ionosphere, J. Geophys. Res. 71, No. 11, 2840-2842.

Baker, D. M., K. Davies, and L. Grimes (1966), Observations of sudden frequency deviations at widely separated places, Nature 210, No. 5033, 253-255.

Bowen, P. J., K. Norman, K. A. Pounds, P. W. Sanford, and A. P. Willmore (1964), Measurements of the solar spectrum in the wavelength band 4-14 Å, Proc. Roy. Soc. of London, Ser. A, 281, No. 1387, 538-552.

Chan, K. L. and O. G. Villard, Jr. (1963), Sudden frequency deviations induced by solar flares, J. Geophys. Res. 68, No. 10, 3197-3224.

Chubb, T. A., H. Friedman, and R. W. Kreplin (1964), Spectrum of solar X-ray emission from 2-20 kev during subflare activity, Space Research IV, ed. P. Muller, 759-768 (North-Holland Publishing Co., Amsterdam).

Conner, J. P., W. D. Evans, M. D. Montgomery, S. Singer, and E. E. Stogsdill (1964), Solar flare X-ray emission measurements and plasma observations at 10^5 km, Space Research V, ed. D. G. King-Hele, P. Muller, and G. Righini, 546-563 (North-Holland Publishing Co., Amsterdam).

Covington, A. E. and G. A. Harvey (1958) Impulsive and long-enduring sudden enhancements of solar radio emission at 10 centimeter wavelength, J. Roy. Astron. Soc. Canada, 52, No. 4, 161-166.

Davies, K. and D. M. Baker (1966), On frequency variations of ionospherically propagated HF radio signals, Radio Sci., 1 (New Series), No. 5, 545-556.

Davies, K., J. M. Watts, and D. H. Zacharisen (1962), A study of F2 layer effects as observed with a Doppler technique, J. Geophys. Res. 67, No. 2, 601-609.

Donnelly, R. F. (1966), An Investigation of Sudden Frequency Deviations Due to the Immediate Ionospheric Effects of Solar Flares, PhD Thesis, University of Illinois.

Friedman, H. (1964), Solar X-ray emission--NRL results, AAS-NASA Symposium on the Physics of Solar Flares, ed. W. N. Hess, NASA SP-50, 147-157, (U.S. Government Printing Office, Washington, D.C.).

Harvey, G. A. (1964), Some relationships between 10.7 centimeter solar noise bursts, flares and short-wave fadeouts, Astrophys. J. 139, No. 1, 16-44.

Kanellakos, D. P., K. L. Chan, and O. G. Villard, Jr. (1962), On the altitude at which some solar flare ionization is released, J. Geophys. Res. 67, No. 5, 1795-1804.

Kundu, M. R. (1965), Solar Radio Astronomy, Chapter 13 (Interscience Publishers, New York).

Pounds, K. A. (1965), Recent solar X-ray studies in the United Kingdom, Annales d'Astrophysique 28, No. 1, 132-145.

Smith, L. G., C. A. Accardo, L. H. Weeks, and P. J. McKinnon (1965), Measurements in the ionosphere during the solar eclipse of July 20, 1963, J. Atmos. Terrest. Phys. 27, No. 7, 803-829.

Tanaka, H. and T. Kakinuma (1958), Observations of solar radio emission at microwave frequencies, Proc. Res. Inst. Atmospherics, Nagoya University, Japan, 5, 81.

Watts, J. M. and K. Davies (1960), Rapid frequency analysis of fading radio signals, J. Geophys. Res. 65, No. 8, 2295-2301.

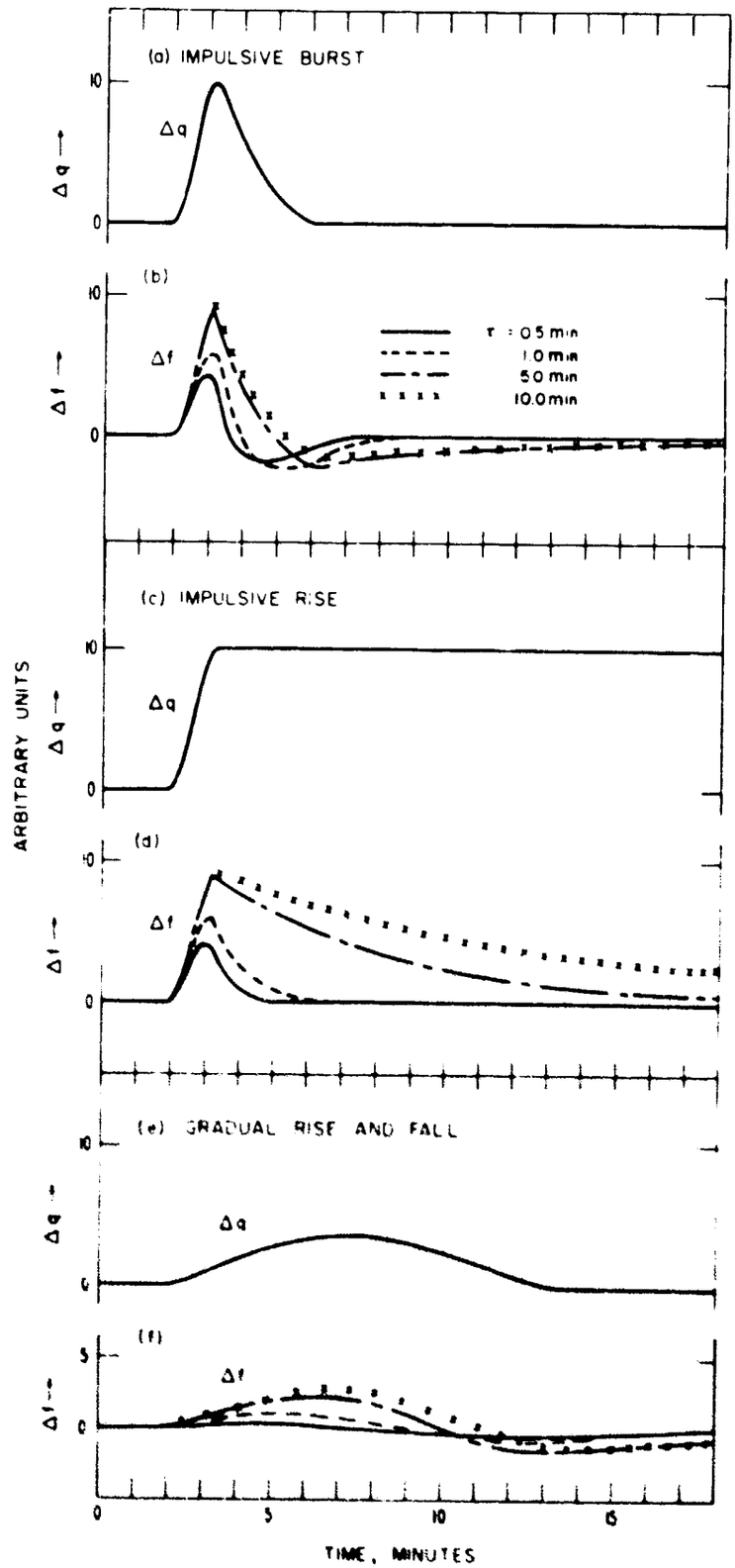

Fig. 1 Simple models of the enhancement of electron production rate and the resulting frequency deviations for effective relaxation times of 0.5, 1, 5, and 10 minutes.

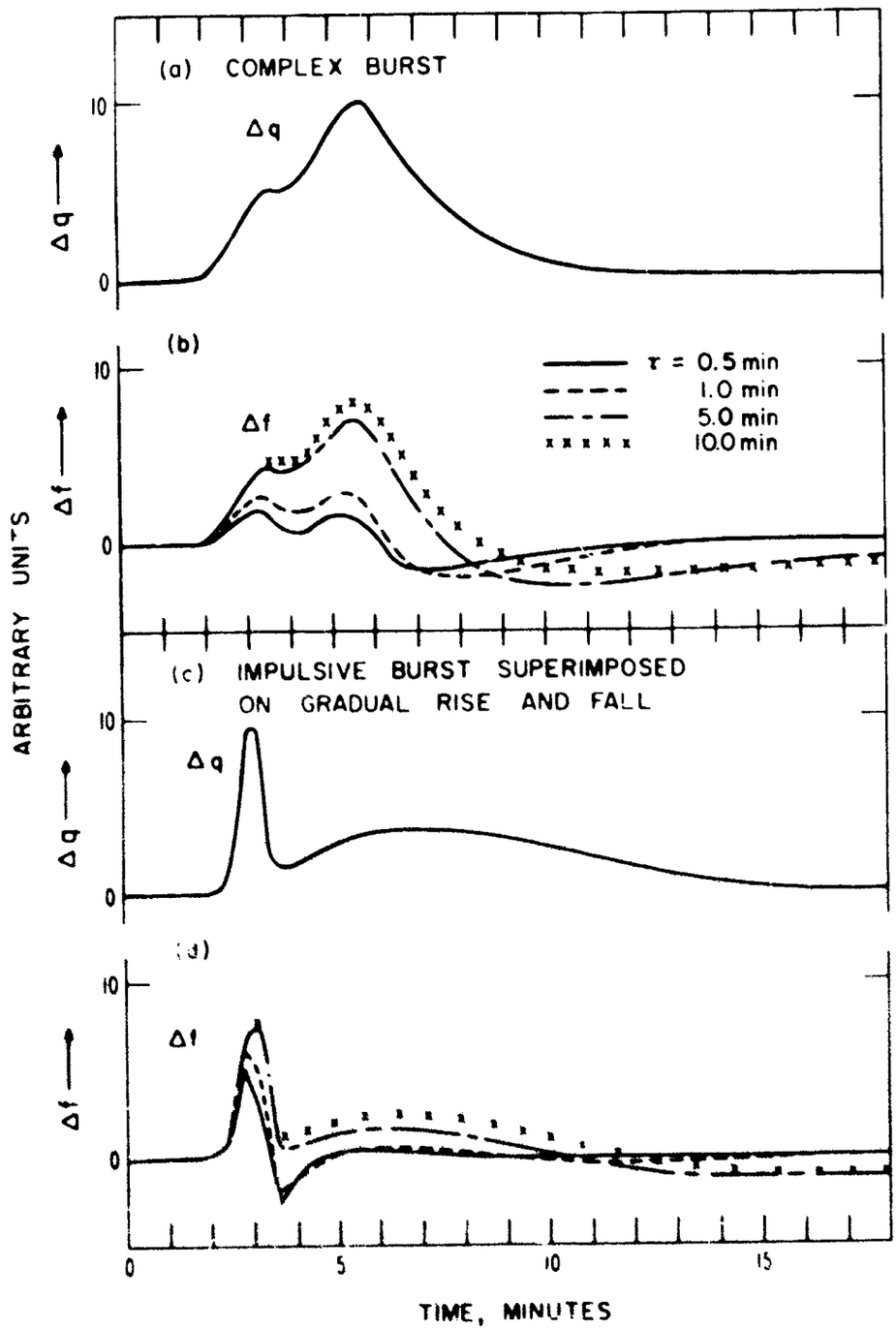

Fig. 4. Complex models of the enhancement of electron production rate and the resulting frequency deviations for effective relaxation times of 0.5, 1.0, 5.0, and 10 minutes.

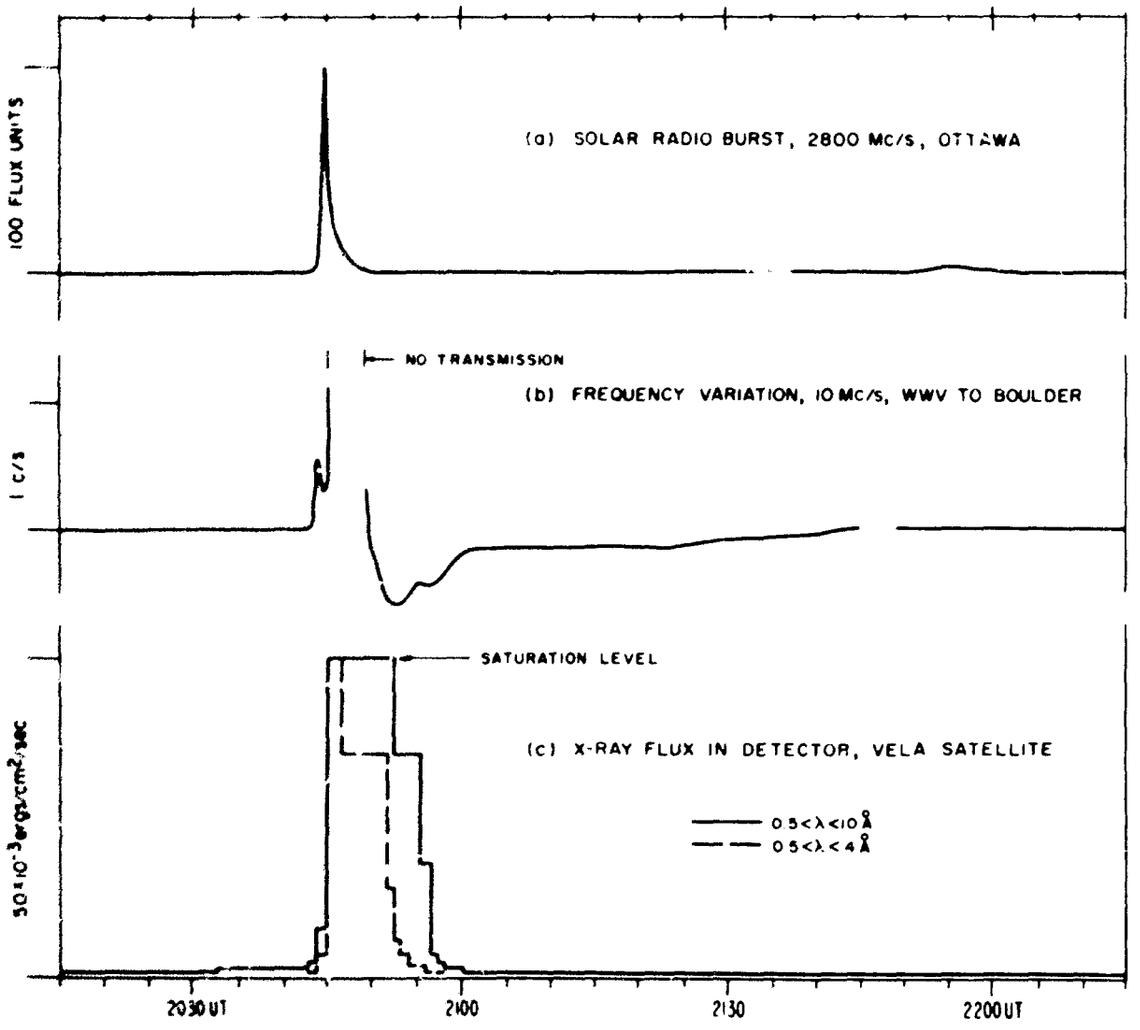

Fig. 3 The solar radio burst (a), frequency variation (b), and solar X-ray burst (c) for the event of 18 October 1963 (2045 U.T.). All scales are linear.

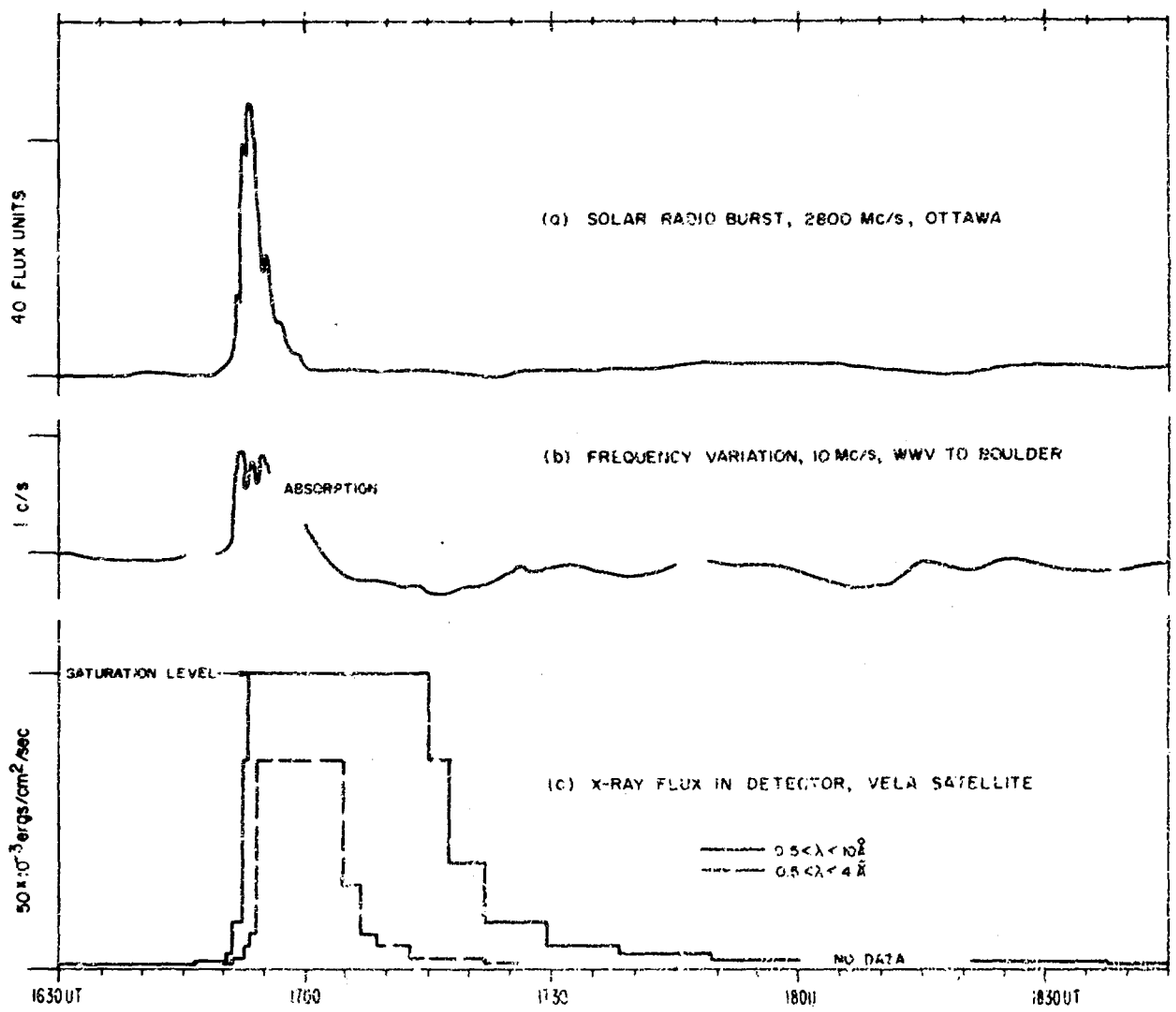

Fig. 4 The solar radio burst (a), frequency variation (b), and solar X-ray burst (c) for the event of 19 October 1963 (1650 U.T.). All scales are linear.

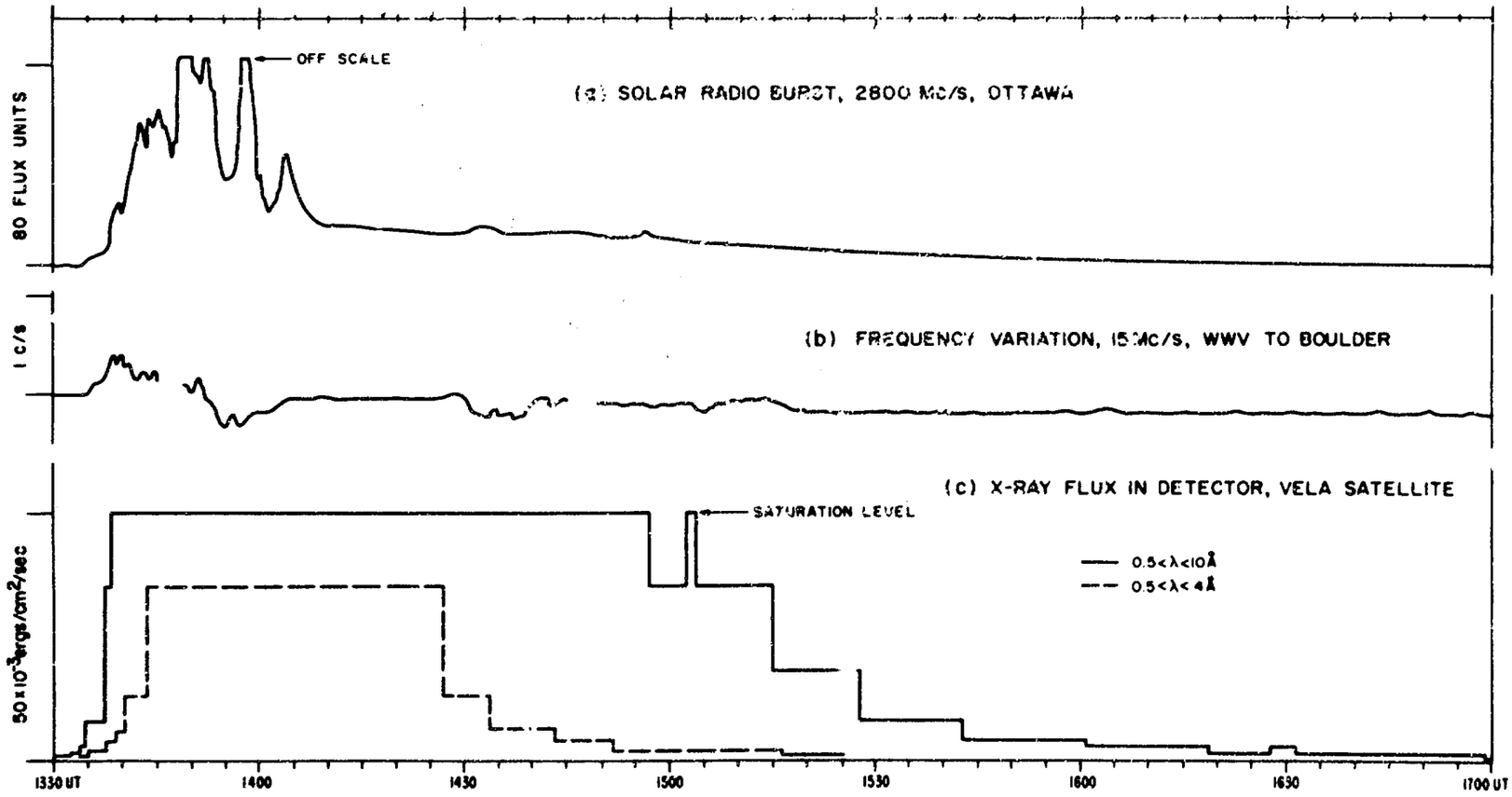

Fig. 5 The solar radio burst (a), frequency variation (b), and solar X-ray burst (c) for the event of 22 October 1963 (1330 U.T.). All scales are linear.

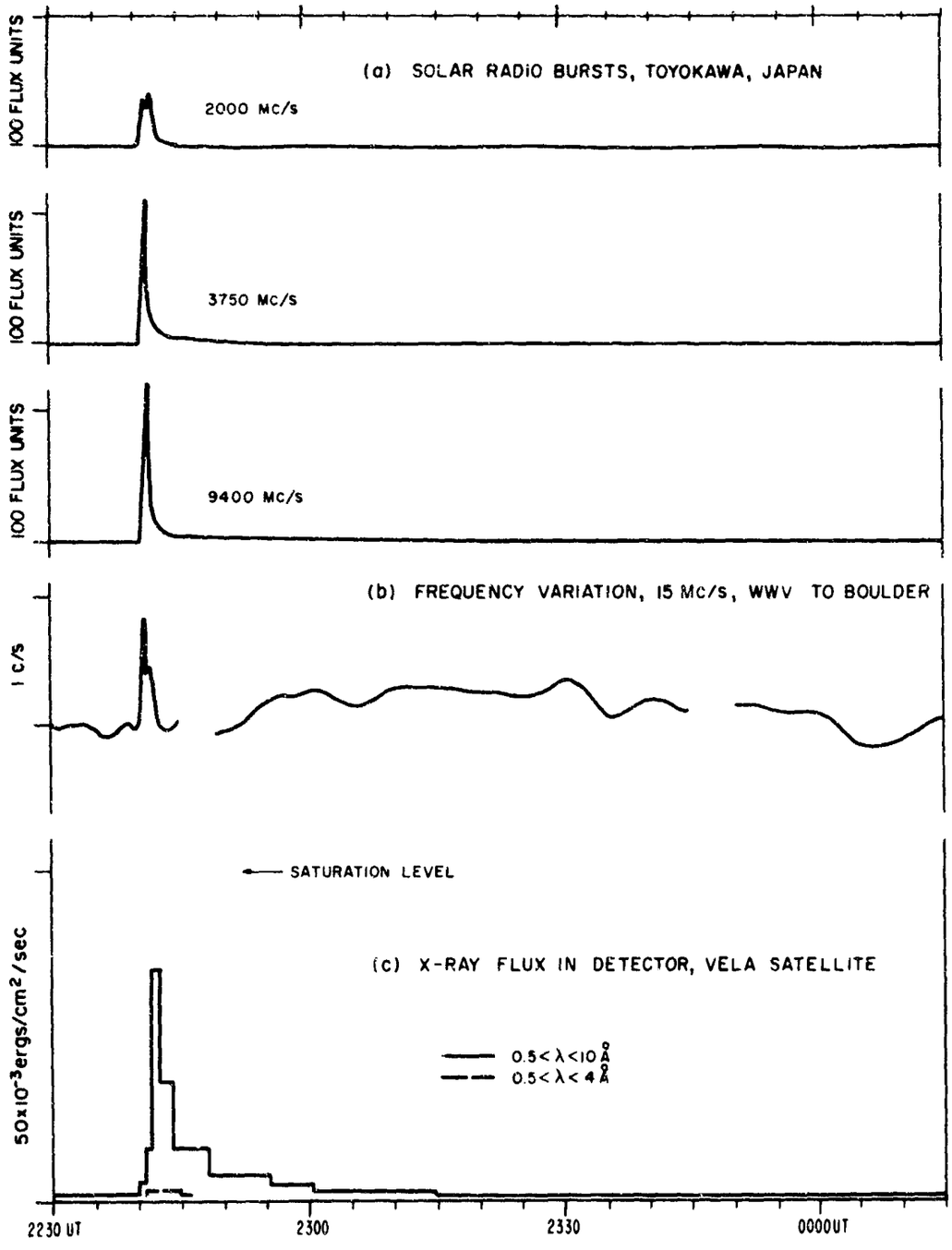

Fig. 6 The solar radio burst (a), frequency variation (b), and solar X-ray burst (c) for the event of 22 October 1963 (2240 U.T.). All scales are linear.

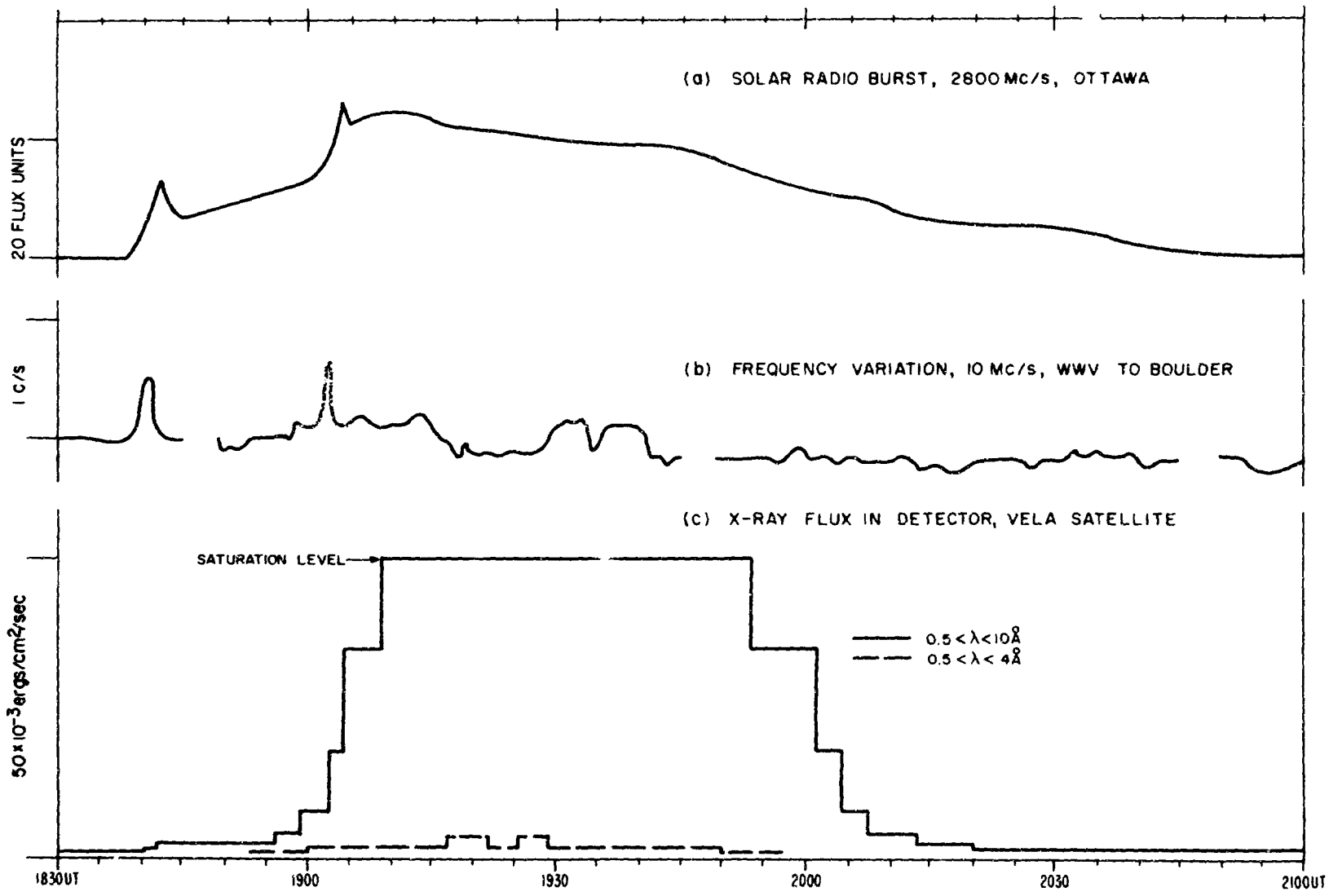

Fig. 7 The solar radio burst (a), frequency variation (b), and solar X-ray burst (c) for the event of 26 October 1963 (1840 U.T.). All scales are linear.

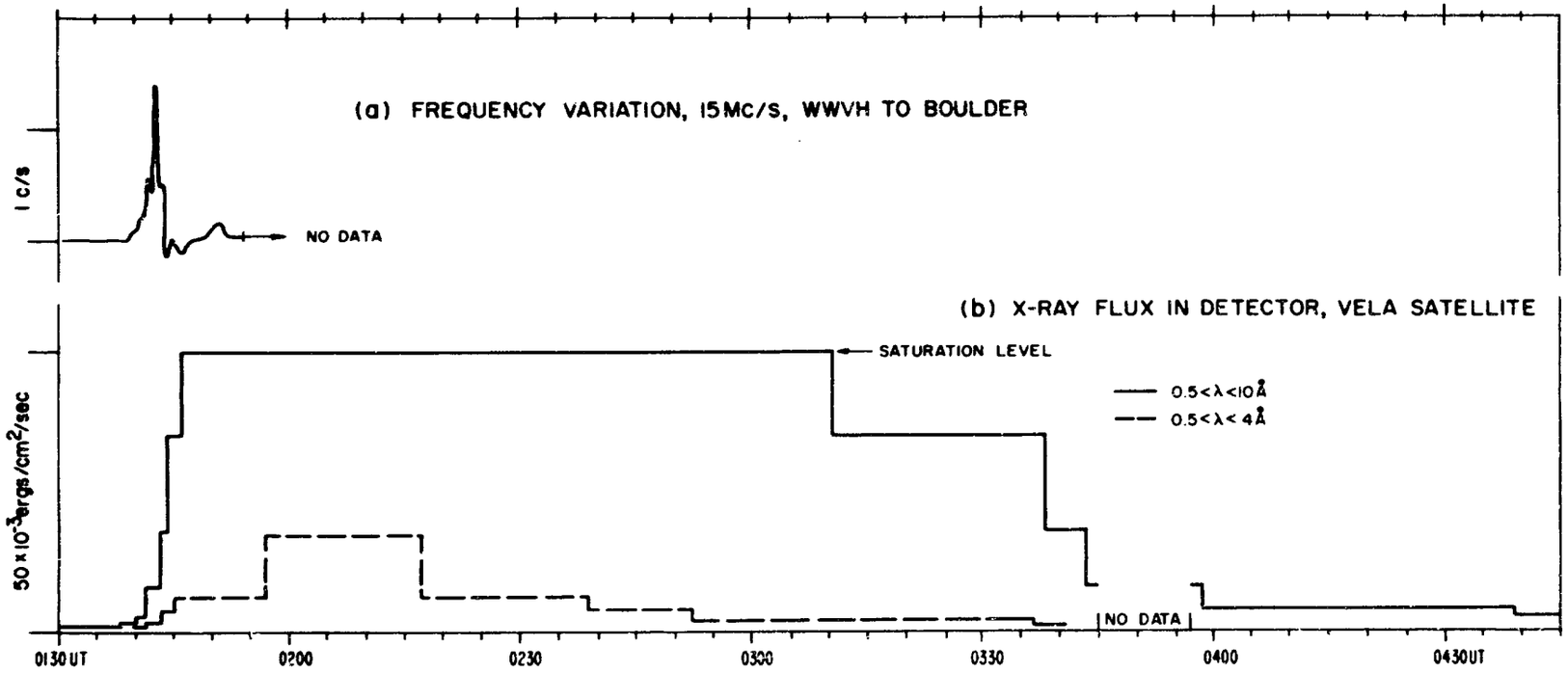

Fig. 8 The frequency deviation and solar X-ray burst for the event of 28 October 1963 (0140 U.T.). All scales are linear.

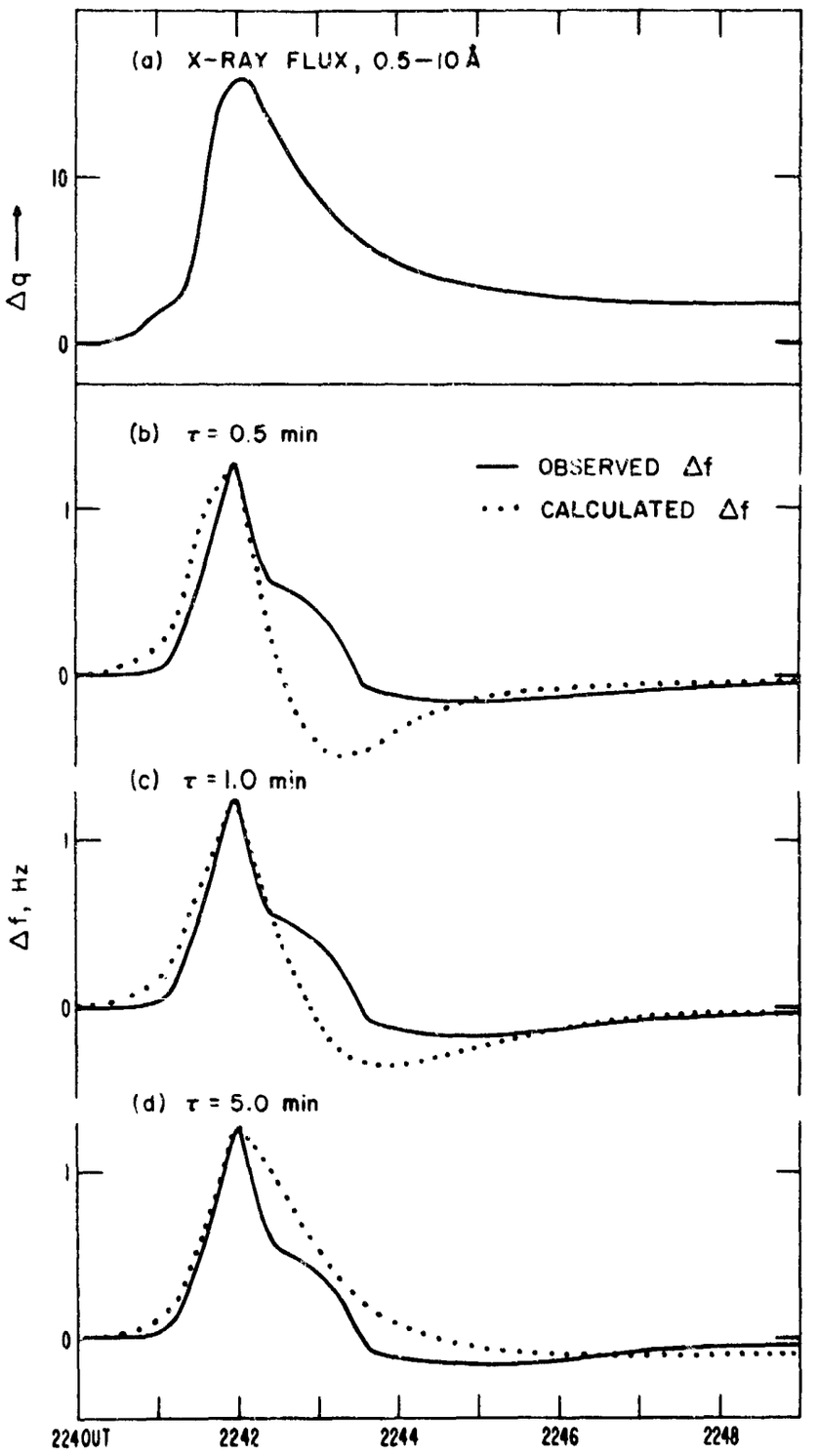

Fig. 9 The 0.5- to 10-Å X-ray flux (a) and the synthesized (dotted) and observed (solid line) frequency variations (b), (c), and (d) for the event of 22 October 1963 (2240 U.T.). The peaks of the synthesized and observed frequency variations have been normalized and aligned.

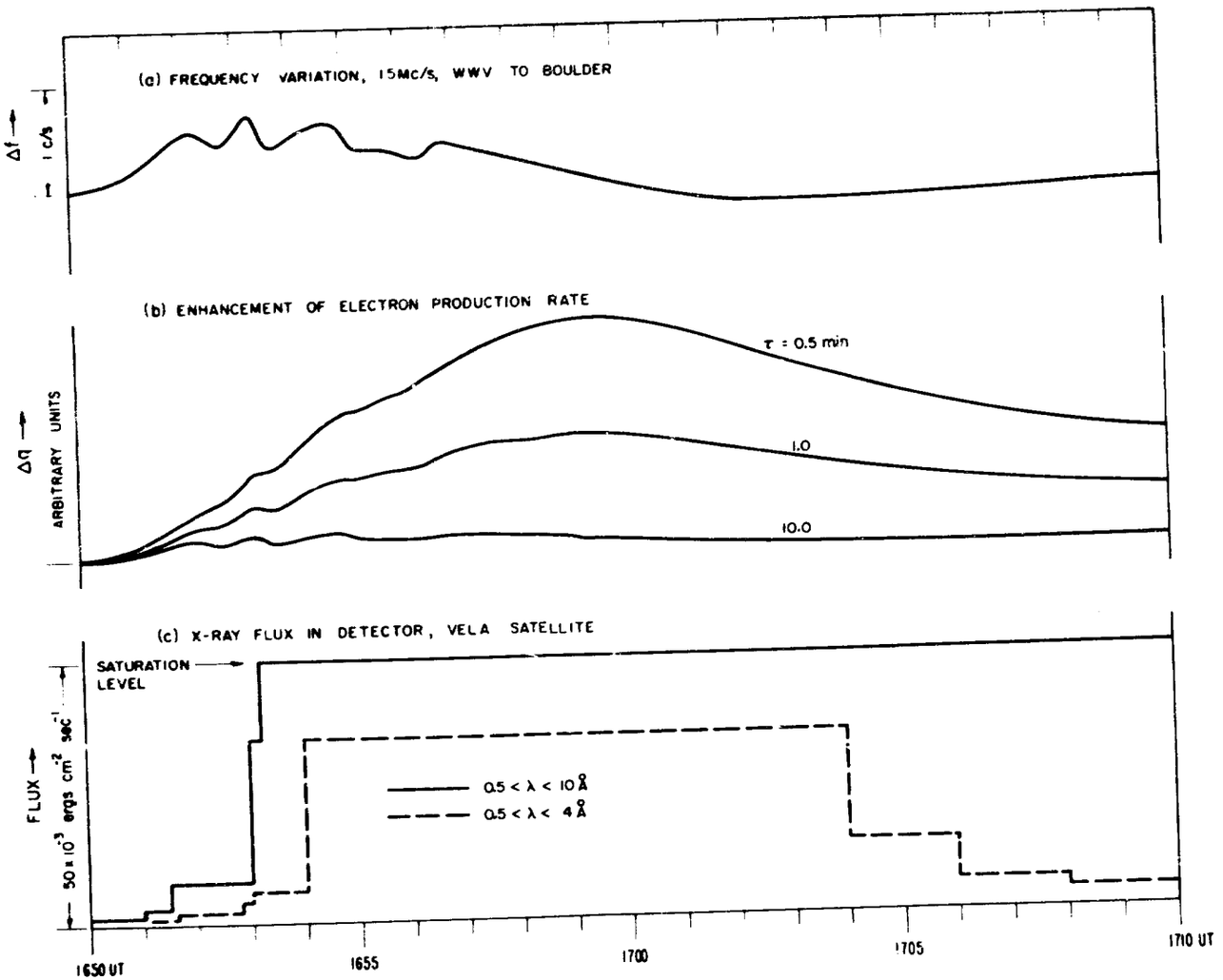

Fig. 10 The observed frequency variation (a) and X-ray burst (c) and the calculated enhancement of the electron production rate for the event of 19 October 1963 (1650 U.T.). All scales are linear.

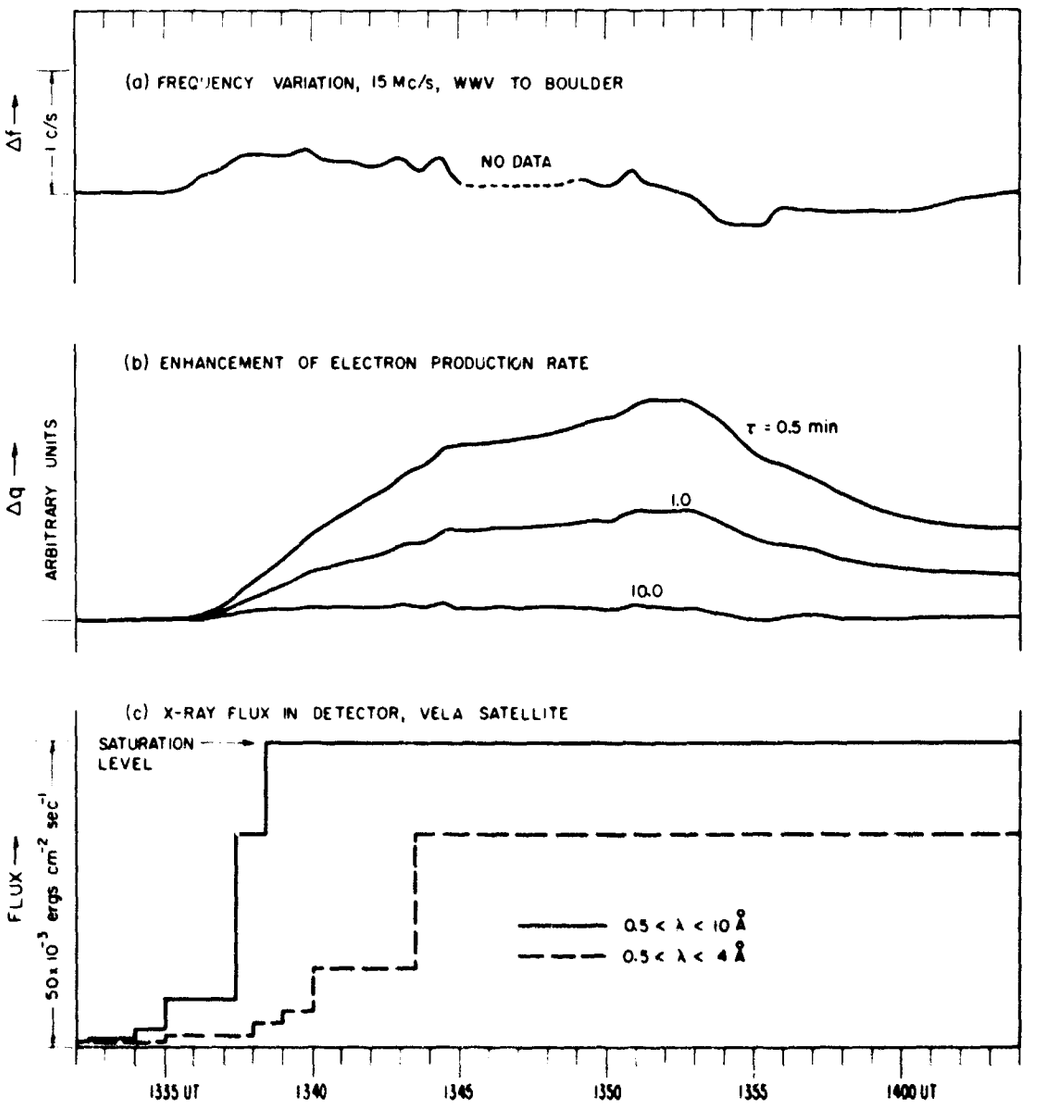

Fig. 11 The observed frequency variation (a) and X-ray burst (c) and the calculated enhancement of the electron production rate for the event of 22 October 1963 (1330 U.T.). All scales are linear.

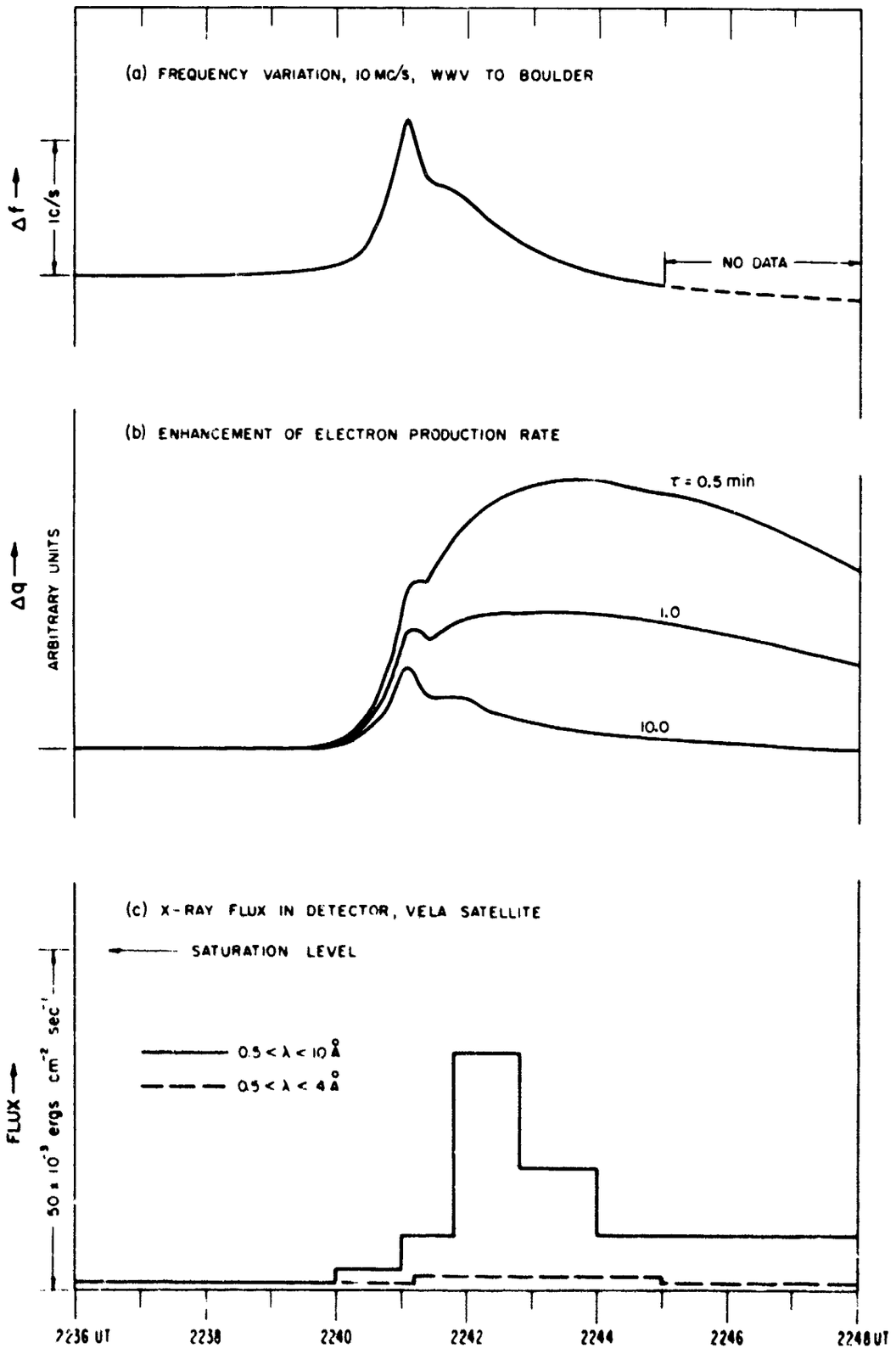

Fig. 12 The observed frequency variation (a) and X-ray burst (c) and the calculated enhancement of the electron production rate for the event of 22 October 1963 (2240 U.T.). All scales are linear.

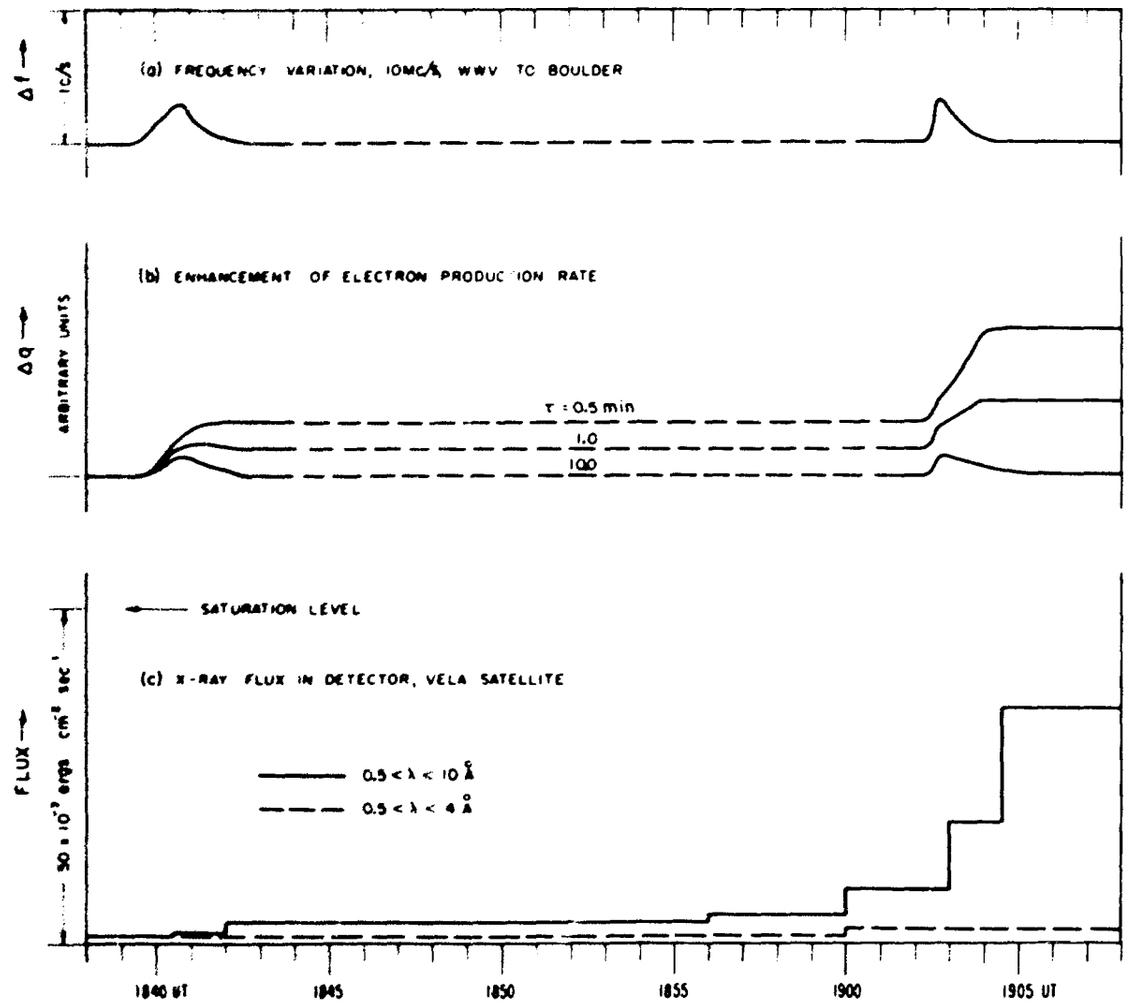

Fig. 13 The observed frequency variation (a) and X-ray burst (c) and the calculated enhancement of the electron production rate for the event of 26 October 1963 (1840 U.T.). The broken lines indicate smoothing of the data. All scales are linear.

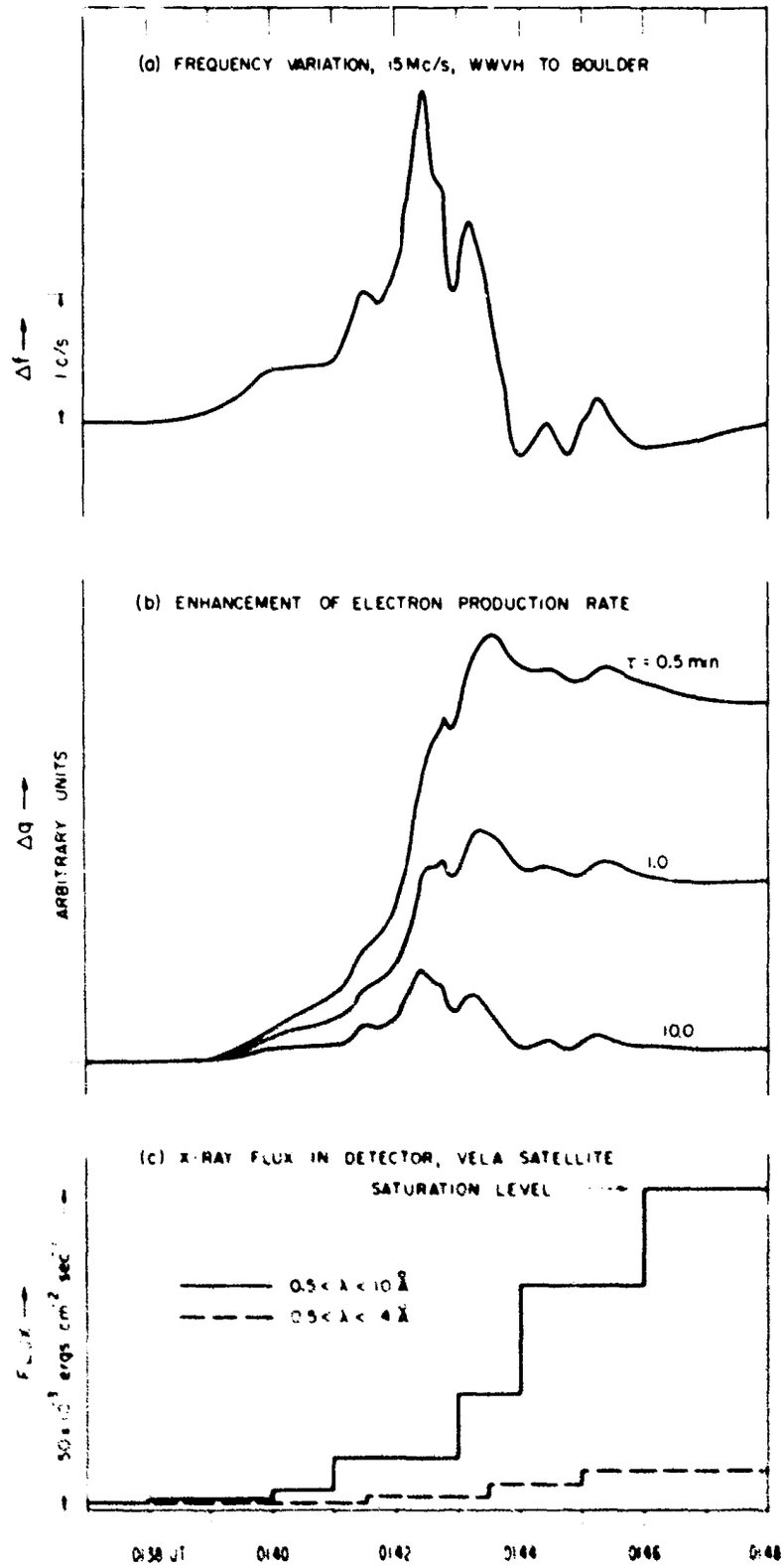

Fig. 1. The observed frequency variation (a) and X-ray burst (c) and the calculated enhancement of the electron production rate for the event of 20 October 1966 (Universal Time). All scales are linear.